Oxygen in silicon: Switch in the diffusion-mediated mechanism

Dilyara Timerkaeva,* Damien Caliste, Thierry Deutsch, and Pascal Pochet*
Laboratoire de Simulation Atomistique (L_Sim), MEM, INAC, CEA, 38054 Grenoble Cedex 9, France
and Université Grenoble Alpes, CS 40700, 38058 Grenoble Cedex, France
(Received 13 October 2016; revised manuscript received 14 October 2017; published 21 November 2017)

The impact of a heavy doping on oxygen diffusion at 350 °C−700 °C is widely discussed in literature, however, the retardation/enhancement mechanisms remains unclear at that temperature range. In this paper, we study the impact of heavy doping on the oxygen diffusion coefficient in silicon by using density functional theory calculations. While it is known that the lowering of temperature induces a switch in the diffusion mechanism from monomer mediated diffusion to dimer one, we have discovered that the reported enhanced oxygen diffusion in *p*-doped silicon is driven by a switch back from the dimer to monomer. We base our claim on extensive calculations of both pre-exponential factors and activation energies in various doping and stress conditions. We show that the stress has a negligible effect and we attribute the switch back to monomer diffusion at low temperatures in *p*-doped materials, to a charge assisted mechanism that reduces the migration energy of the monomer of 0.4 eV, while the diffusion rate is kept high thanks to the pre-exponential factor. We also provide comparisons to *n*-doped and isovalent cases.

DOI: 10.1103/PhysRevB.96.195306

I. INTRODUCTION

The production of a pure and homogeneous monocrystal of silicon is still relatively expensive. The industrial crystal growth methods lead to inclusion of impurities into a silicon crystal, namely light elements, metallic elements, and dopants. The impurities interacting with each other, with dopants and with self-interstitials or vacancies [1], sometimes result in substantial changes of the formal material's properties.

Oxygen is a particular impurity as it is nearly always present in crystalline silicon in concentrations of 10^{17}–10^{18} cm^{-3} [2]. Its impact on silicon-based devices is ambiguous. On one hand, it does not affect the electrical properties of silicon; it improves the mechanical strength of the crystal, and in the form of precipitates it getters the undesired metallic impurities [3]. On the other hand, the so-called thermal donors [4,5] presence is caused by the formation of oxygen agglomerates. Moreover, some oxygen containing defects (such as V-O, C-O, or B-O complexes) act as recombination centers and reduce the solar cell efficiency [6,7]. In particular, the boron-oxygen complexes are responsible for the ligh-induced degradation of solar cells [6,8–10]. Both the exact composition of the complex and its formation mechanism remain debated [9–12], although the method to passivate the complex activity was already defined [13]. The oxygen mobility, and thus its ability to agglomerate or to form complexes, depends on the temperature range, as well as on the concentration of dopants and impurities.

A. Temperature dependence of oxygen diffusion

In low doped silicon, one can distinguish two temperature ranges: (i) the high temperatures, above 700 °C up to melting temperature and (ii) the low temperatures, 350 °C−700 °C. At high temperatures, we observe the so-called "normal" diffusion, which diffusion coefficient can be described by the following empirical expression [14]:

$$D(O) = 0.13 \exp\left(-\frac{2.53\ \text{eV}}{kT}\right) \text{cm}^2\,\text{s}^{-1}. \quad (1)$$

In this case, an interstitial oxygen monomer is the particle responsible for oxygen transport, the so-called "mediator."

At low temperatures, an "enhanced" oxygen diffusion is observed. It is due to a switch in the diffusion species. The oxygen dimer is thought to become the primary diffusing species in this regime. The enhancement is associated with an activation energy of 1.5 eV [15–17], however, some recent experiments suggest an activation energy of 2.0 eV [18,19].

B. Doping and impurity affected oxygen diffusion

While the oxygen diffusivity is not affected by low doping rates, it is sensitive to the high doping concentrations ($>10^{18}$–10^{21} cm^{-3}) [20–23], but also to the influence of hydrogen and metallic incorporation [24–26]. The numerous experimental evidences gathered during the past two decades have revealed certain trends. At high temperatures, heavy doping leads to either very weak or no impact on oxygen diffusion and precipitation kinetics [23,27,28], whereas at low temperatures, experiments show contradictory trends.

As far as the effect depends on the doping type, three main groups of dopants can be distinguished: *p*-type, *n*-type, and isovalent dopants. Most of the studies suggests an enhanced oxygen diffusion in heavily doped *p*-type silicon. The first indirect evidence was an observation of the enhanced thermal donor formation as reported by Wada *et al.* [29]. Another evidence has been provided by recent dislocation locking technique (DLT) experiments. DLT measurements have suggested an increase of the oxygen transport by a factor of at least 8, compared to low doped materials [20,21]. The enhanced kinetics of the oxygen precipitation in heavily B-doped materials [23] supports the enhanced oxygen diffusivity. However, some earlier SIMS out-diffusion profiles have shown a reduced oxygen diffusivity in heavily B-doped samples at 600 °C−800 °C by a factor of 2 to 5 [30]. In other words,

*Corresponding authors: dtimerkaeva@gmail.com; Pascal.Pochet@cea.fr

the experiments have suggested an opposite effect of heavy B doping on the oxygen transport in the low temperature range. Recent study performed by Torigoe *et al.* [22] revealed that the oxygen diffusion coefficient is proportional to the square root of B concentration at 750 °C−1000 °C temperature range.

There are few evidences of reduced oxygen diffusion in heavily n-type doping at low temperature range. Phosphorus doping reduces the thermal donor formation according to Wada *et al.* [29]. Both heavily arsenic-doped and antimony-doped samples slow the oxygen diffusion as revealed by Takeno *et al.* [30], by increasing its migration energy by 0.64–0.68 and 1.4 eV, respectively. Dislocation locking experiments show a slowing down of oxygen diffusivity by a factor of 5 in heavily As-doped silicon [21]. However, no dependence of the diffusivity was found in antimony-doped silicon by means of DLT experiment [20].

Doping with germanium slows the oxygen diffusivity by a factor of 4 according to Zeng *et al.* [21] in the low temperature range. Since stress-induced dichroism technique is only sensitive to the oxygen monomer diffusion, it was shown that the increasing of the germanium content slows more the monomers diffusion at 375 °C [31].

To summarize, p-type, n-type, and isovalent doping impacts the oxygen diffusivity at low temperatures. As it was earlier concluded by Zeng *et al.* [21], experimental evidences suggest that both internal strain and change in Fermi energy level may cause the changes in kinetic properties of oxygen. For example, high germanium content introduces relatively important change in lattice parameter ($\frac{\Delta a}{a} = +7\times10^{-5}$) of silicon without affecting its electrical properties. While high content of p- and n-type dopants changes the Fermi energy level of the crystal. And as it was reviewed above, both cases are known to impact oxygen diffusivity properties.

In the last decades, significant efforts were made in order to understand the mechanisms lying behind the observed changes in oxygen diffusivity. For example, other diffusing complexes, such as VO, Si_iO, molecular O_2 [32], chains of more than three interstitial oxygens [33], were proposed as a diffusing species. Later, it was shown that they can barely be involved in oxygen transport [34,35]. Dimers diffusion in doubly charged state is an alternative for an enhanced transport as proposed by Adey *et al.* [36,37]. However, no signs of charged dimers were yet observed [38]. Another explanation for the enhanced diffusion is the so-called Bourgoin-Corbett mechanism [39–41]. Such mechanism is based on the fact, that the ground-state configuration of the neutral oxygen dimer becomes the saddle point of the doubly charged state, whereas the saddle configuration of the neutral dimer becomes the ground state. This mechanism suggests that the oxygen dimer captures and releases one or two electrons and diffuses with a very low activation barrier or even nearly barrierless, which contradicts the experimental observations.

Recently, we have investigated the oxygen migration barrier (E_m) in the proximity of a dopant with a numerical approach based on density functional theory (DFT) [42]. We have shown that E_m for the oxygen monomer can be reduced due to a charge assisted mechanism in the proximity of a p-type dopant. In its ground state, oxygen is a neutral particle, but by approaching the saddle point, it attracts an unpaired electron from the vicinity of the p dopant. We have shown

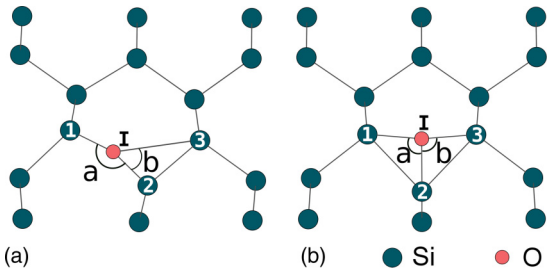

FIG. 1. Oxygen monomer's (a) ground state and (b) transition state schematic configurations. In Table I, $\hat{Si}_{123}$ stands for an angle between Si_1-Si_2 and Si_2-Si_3 bonds.

that the charge assisted mechanism reduces the monomer's migration energy E_m by 0.4 eV. We have suggested that this reduction can accelerate the dimer formation, whereas dimers remain the primary diffusion mediators. Nevertheless, any final conclusion on the effect of this reduction on the oxygen diffusion, requires to calculate the complete diffusion coefficient for both monomers and dimers, and not only the migration barrier. Only such complete calculations can give a clue towards the proper understanding of the underlying processes.

In this paper, we investigate the impact of doping on the diffusivity of both oxygen monomers and dimers. The diffusivity of the migrating species can be described by the diffusion coefficient D and can be expressed in the most general form as

$$D = D_0 \exp\left(-\frac{E_a}{kT}\right). \tag{2}$$

Here, E_a is the activation energy and D_0 is the pre-exponential factor. Both parameters can be calculated from first-principles methods [43,44]. We separately study the effect of strain and the effect of Fermi energy level. We calculate the pre-exponential factor D_0 of the full diffusion coefficient in addition to the activation energy E_a for each considered case. By performing DFT simulations, we show that uniaxial or biaxial strain does not affect the diffusion coefficient value. However, the shift in Fermi level due to incorporation of p- or n-type dopant into the supercell, impacts the diffusion coefficient significantly. In the latter case, dopant atom can be also thought as a source of electrons.

The paper will be organized as following. Firstly, we give the computational methodology employed in this study. Secondly, we will introduce the calculations of diffusion coefficient for monomer and dimer in the unconstrained supercell. Then, we will consider the effect of the strain and of the doping. The obtained diffusion coefficients will be later discussed and compared with existing experimental data.

II. METHODOLOGY

In the case of a simple defect diffusion, such as an interstitial oxygen monomer, the activation energy is equal to the migration energy, i.e., the minimal energy needed to jump to a closest neighboring ground state (GS) through the transition state (TS), see Figs. 1(a) and 1(b): $E_a(A) \equiv E_m(A) = E^{TS} - E^{GS}$. In the case of diffusing defect complex,

such as oxygen dimer, the activation energy also depends on its binding energy E_b and can be expressed as

$$E_a(AB) = E_m(AB) - E_b(AB), \tag{3}$$

with

$$E_b(AB) = -E_{\text{tot}}(N\text{Si}AB) - E_{\text{tot}}(N\text{Si}) + E_{\text{tot}}(N\text{Si}A) + E_{\text{tot}}(N\text{Si}B), \tag{4}$$

where N is the number of Si atoms in the supercell.

The corresponding energies of monomer and dimer configurations were obtained using density functional theory calculations under the spin polarized generalized gradient approximation with Perdew-Burke-Ernzerhof functional [45]. The core electrons have been treated with norm-conserving Hartwigsen-Goedecker-Hutter pseudopotentials [46]. The wavelet based BIGDFT code [47] have been employed. The basis set accuracy was given by a grid spacing of 0.44 Bohr that provides energy values with an accuracy of 20 meV within the given approximations. Fast inertial relaxation engine [48] (FIRE) and direct inversion in interactive subspace (DIIS) [49] force-based optimizers were used to converge to the ground-state and saddle point configurations, respectively [50]. The criterion on forces for geometry optimization was chosen to be smaller than 3×10^{-4} Ha Bohr^{-1}.

The second parameter of Eq. (2), namely the pre-exponential factor, depends on the single jump length d, the number of equivalent paths p and the dimensionality of the space n. Taking into account the random walk theory and the vibrational entropy of the diffusion path as proposed by Vineyard *et al.* [43] one gets the expression for the pre-exponential factor value:

$$D_0 = \frac{d^2 p}{2n} \frac{\prod_i^N \nu_i^{\text{GS}}}{\prod_i^{N-1} \nu_i^{\text{TS}}}. \tag{5}$$

Here, ν_i^{GS} and ν_i^{TS} are the vibrational modes of the ground-state and transition state configurations, respectively. N is the number of the frequency modes, which is equal to $n.M - n$, where n is the space dimensionality and M the number of atoms in the system.

The phonon spectra of the system with a defect was calculated in a frozen-phonon approximation, where only the first shell of defect's neighbors were taken into account in the dynamical matrix. Perfect supercell elements were considered for the rest of the matrix. The increase of the shell size, by inclusion of up to 32 nearest neighbors around the interstitial oxygen defect, leads to a variation in each frequency mode by less than 1.5%. Thus we imply that the first nearest neighbors approximation leads to converged enough results.

The supercell size strongly impacts the results of DFT calculations of point defect studies, as periodic boundary conditions lead to spurious interactions between periodical images of the defect. A 192 Si atoms supercell was employed for the investigation of the impact of strain on diffusing properties, with a Monkhorst-Pack grid of $1\times1\times3$ for the k-point sampling. X and Y axes of the supercell are collinear with $\langle110\rangle$ and $\langle1 = 10\rangle$ crystallographic directions, while Z axis is collinear with $\langle001\rangle$ direction. That orientation allows to apply uniaxial and biaxial strain along the migration path of interstitial oxygen monomer and dimer. Strains ranging from -1.0% to $+1.0\%$ have been applied. The supercell was allowed to relax along unconstrained axes. Then the diffusing species were introduced in the supercell and the calculations of migration energy as well as the pre-exponential factor value were performed.

TABLE I. Geometry parameters of the oxygen monomer configurations (see Fig. 1 for the schemes). The length values are in Bohrs, the angles are in degrees. For reference, the calculation parameters we have used give a Si-Si bond length of 4.468 Bohr.

doping	conf.	$\hat{a}$	$\hat{b}$	$\hat{\text{Si}}_{123}$	Si_1-O	Si_2-O	Si_3-O	Si_1-Si_2	Si_2-Si_3
pristine	GS	161.9	52.0	103.9	3.069	3.068	5.586	6.061	4.415
B	GS	162.0	51.9	103.9	3.068	3.068	5.589	6.060	4.416
Ge	GS	162.1	51.9	103.9	3.068	3.068	5.590	6.061	4.414
As	GS	162.1	51.9	103.9	3.068	3.068	5.590	6.061	4.415
pristine	TS	94.9	94.0	87.2	3.472	3.374	3.487	5.045	5.018
B	TS	101.2	94.8	85.9	3.528	3.304	3.611	5.280	5.096
Ge	TS	94.5	94.5	87.0	3.481	3.581	4.477	5.041	5.036
As	TS	93.4	91.7	91.7	3.544	3.294	3.572	4.979	4.931

To study the impact of doping on oxygen migrating properties, we used a 512 Si atoms supercell. First, we incorporated a substitutional dopant to the supercell and performed a full relaxation of the atomic positions within the supercell. Then an oxygen atom was introduced in the middle of the area elastically unperturbed by the dopant presence. That allowed avoiding the elastic interaction between dopant and oxygen atoms and corresponds to a distance of 15 Å.

To further investigate the charge assisted diffusion, the nudged elastic band (NEB) algorithm has been employed for a few representative cases in a 216 Si supercell. NEB paths of 41 images were converged within the convergence criteria of 0.005 Ha/Bohr on forces, which are perpendicular to the path direction.

III. RESULTS

A. Instrinsic silicon

1. Diffusion coefficient of monomer

We start by describing the isolated interstitial oxygen diffusion, which mainly occurs at high temperatures. The interstitial oxygen impurity is situated between two neighboring Si atoms and is covalently bonded to them as illustrated in Fig. 1(a). The diffusion proceeds in one of the three equivalent $\langle110\rangle$ directions. Thus we consider the number of equivalent paths equal to six $p = 6$. The oxygen atom jumps to the neighboring bond-centered site by passing through the transition state. The latter is a highly symmetric threefold coordinated configuration as illustrated in Fig. 1(a). The corresponding jump length was measured to be $d = 2.83$ Bohr. The optimized structural parameters for ground state and transition state are listed in Table I.

The calculated migration energy and pre-exponential factor are listed in Table II together with geometry parameters of a single jump used in the calculations. The calculated diffusion coefficient can be expressed as

$$D_O^{\text{calc.}} = 0.029 \exp -\frac{2.40}{kT} \text{ cm}^2\,\text{s}^{-1}. \tag{6}$$

TABLE II. The calculated migration energies (E_m), binding energies (E_b), activation energies ($E_a = E_m - E_b$), and pre-exponential factors (D_0) for oxygen monomer's and dimer's diffusion. The low temperature pre-exponential factor $D^{\rm lt}_{0\rm eff}$ is described by Eq. (8) and depends on the oxygen monomers concentration.

	calculations (this work)						experiment [14,51]	
	[O] ($\rm cm^{-3}$)	E_m (eV)	E_b (eV)	E_a (eV)	D_0 ($\frac{\rm cm^2}{s}$)	$D^{\rm lt}_{0\rm eff}$ ($\frac{\rm cm^2}{s}$)	E_a (eV)	D_0 ($\frac{\rm cm^2}{s}$)
monomer	–	2.41	–	2.41	0.029	–	2.53	0.13
dimer	10^{18}	1.62	0.14	1.48	0.013	7.63×10^{-7}	1.55	2.16×10^{-6}

Figure 2 reports the calculated Arrhenius plot of diffusion coefficient together with experimental data from Ref. [14]. The fit of experimental points [14] [described by Eq. (1)] is plotted with a dashed black line, whereas plain red line reproduces the results of the present calculations [Eq. (6)]. The calculated diffusion coefficient lies excellently on the measured experimental points.

2. *Diffusion coefficient of dimer*

In literature, it was suggested that dimers migrate at temperatures <700 °C [16,17,35,52]. Murin *et al.* [53] have provided the experimental evidence for fast diffusing dimer via IR absorption experiments. According to numerous first-principles calculations [33,54], the dimers are two oxygen monomers placed on neighboring Si-Si bonds, the so-called staggered configuration, as illustrated in Fig. 3(a). In the present study, such configuration was found to be the most stable with respect to other dimer geometries. Here, the corresponding binding energy was obtained as follows:

$$E_b(O_2) = -E(512\text{Si} + O_{2i}) - E(512\text{Si}) + 2E(512\text{Si} + O_i). \quad (7)$$

The expression gives a value of 0.14 eV, while experiment suggests 0.3 eV [53]. The discrepancy of 0.16 eV can have multiple reasons, one of the main is the choice of pseudopotentials.

The dimer diffuses through the square form [see Fig. 3(b)] with a migration energy of 1.62 eV. Then, a nearly barrierless rotation around Si-Si bonds is required to continue the diffusion in the same direction. The activation energy, obtained using Eq. (3), is therefore equal to 1.48 eV, which is in an excellent agreement with the experimental data listed in Table II.

Once the dimer is formed, it preferably diffuses forward or backward along the particular ⟨110⟩ direction because its reorientation to another (110) plane is an energetically unfavorable procedure. According to Lee *et al.* [33], it is as costly as an interstitial monomer migration. So we considered this process as rarely occurring and thus negligible at low temperature regime. This is why to calculate the pre-exponential factor value $D_0(O_2)$, we take the number of possible equivalent directions $p = 2$ and the single jump length $d = 2.46$ Bohr.

However, the effective diffusion coefficient at low temperatures depends not only on oxygen dimer diffusion coefficient, but also on the overall oxygen concentration and binding energy of a dimer [20,53]. It can be expressed as

$$D^{\rm lt}_{\rm eff} \approx D(O_i) + 2\frac{C(O_i)}{N_{SO}}\frac{g_2}{g_1}D_0[O_{i2}]\exp\left(-\frac{E_m - E_b}{kT}\right) \approx D^{\rm lt}_{0\rm eff}\exp\left(-\frac{E^{\rm lt}_a}{kT}\right), \quad (8)$$

where $g_1 = 4$ and $g_2 = 12$ and represent possible sites of O_i and O_{i2} in a unit cell, N_{SO} is a density of possible sites of O_i. At the low temperature ("lt") regime, the impact of monomers diffusion to the oxygen transport can be neglected, as the migration energy of a monomer is much higher than that of a dimer. Therefore the low temperature effective pre-exponential factor can be expressed as $D^{\rm lt}_{0\rm eff} = 2\frac{C(O_i)}{N_{SO}}\frac{g_2}{g_1}D_0(O_{i2})$.

Assuming the initial oxygen concentration being $10^{18}\,\rm cm^{-3}$, the calculated $D^{\rm lt}_{0\rm eff}$ is $7.63\times10^{-7}\,\rm cm^2\,s^{-1}$. Figure 4 shows the Arrhenius plot of calculated diffusion coefficient for the oxygen dimer at low temperature range (plain red line) that is compared with DLTS experimental data

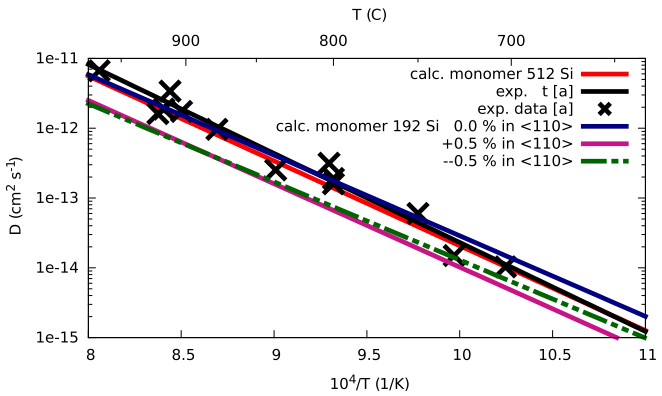

FIG. 2. Arrhenius plot of the oxygen monomer's diffusion coefficient calculated for the fully relaxed and strained supercells. [a] Reference [14].

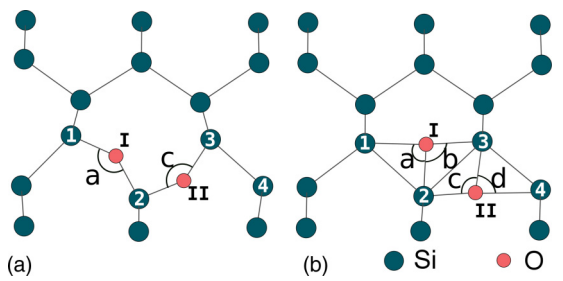

FIG. 3. Oxygen dimer's (a) ground-state and (b) transition state configurations. In Table III, $\hat{\rm Si}_{123}$ and $\hat{\rm Si}_{234}$ angles are defined in the same manner as in Fig. 1.

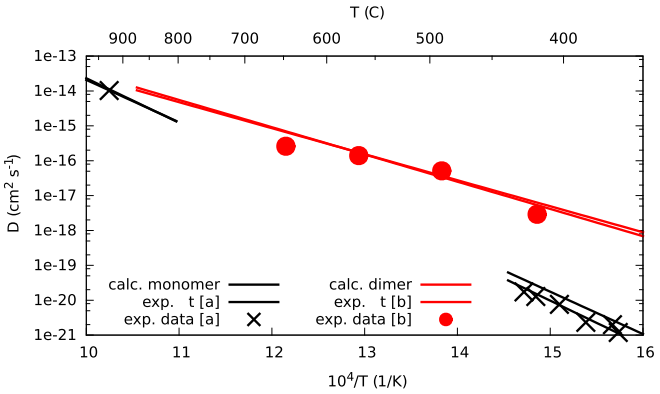

FIG. 4. Oxygen dimer diffusion coefficient. [a] Reference [14]. Below 450 °C, the stress-induced dichroism experiments, which are sensitive only to monomers diffusion, are well described by the extrapolation of the high temperature diffusion coefficient. These data also agree with the calculated diffusion coefficient for monomers. [b] Reference [17]. The experimental data (red circles) are an effective oxygen diffusivity. These data agree with the calculated diffusion coefficient for dimers.

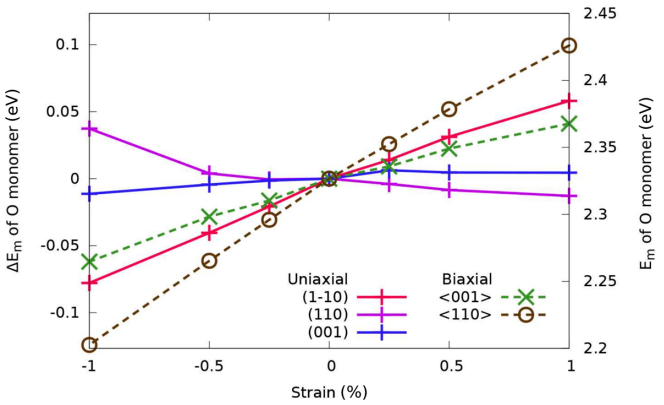

FIG. 5. The effect of the uniaxial and biaxial strains. Oxygen monomer migrates along $(1\bar{1}0)$ direction and stays in ⟨110⟩ plane. The variation in energy is less than 0.1 eV.

fit from Refs. [17,20,51] (dashed red line). Our results are in a fair agreement with the experimental fit.

Once we reproduced the diffusing properties of oxygen in the unperturbed pristine Si, we can consider how heavy doping can affect oxygen diffusing properties. We will consider the two hypothesis proposed in literature for the enhanced and retarded oxygen diffusion: the effect of strain (Sec. III A 3) and the effect of the Fermi energy change due to the high doping concentration (Sec. III B) on the oxygen diffusion features.

3. *Strain effect*

The first hypothesis to check theoretically is the effect of strain on the oxygen diffusion coefficient. We remind that this calculations have been performed in a 192 Si atoms supercell, which frame of references can be obtained through rotation by 45 °C around the Z axis of a 216 Si atoms supercell. In the new frame of references, we let the monomer locate and diffuse in ⟨110⟩ crystallographic plane along the $(1\bar{1}0)$ direction. The effect of applied strain on oxygen monomer migration energy is illustrated in Fig. 5.

External compressive strain tends to reduce the migration energy, while the external tensile strain tends to increase it almost in all cases except when it is uniaxially applied in (110) direction, *i.e.* perpendicular to the diffusion direction. The effect of uniaxial strain is maximum when it is applied along the migration direction. A variation of less than 0.1 eV is obtained for 1% deformation. The biaxial strain applied in diffusion plane gives a variation of 0.15 eV for the monomer migration energy.

However, a strain of ±1.0% can barely be realized due to the dopant's presence. A change of -7×10^{-3}% was observed by Zeng *et al.* [21] in heavily Ge-doped samples, while for heavy doping with other elements the average absolute strain is below 8×10^{-4}%. Thus we conclude that neither uniaxial nor biaxial strain will cause noticeable changes in the migration energy of the monomer.

Table IV lists the calculated pre-exponential factor and migration energy parameters for ±0.5% biaxial ⟨110⟩ strain. The temperature evolution of diffusion coefficient for these cases is shown in Fig. 2. Both compressive and tensile biaxial strain lead to a reduced monomer diffusivity. However, the change in diffusivity will be negligible for strains induced by doping only. Same trends were obtained for dimer's diffusivity. Hence, strains, induced by heavy doping, can cause no effect on both monomer and dimer diffusivity. We can conclude that neither monomer's nor dimer's migration energies can be affected by external strain, as well as the monomer's pre-exponential factor.

B. Doped silicon

We can rule out the effect of external strain to explain the reported enhancement or retardation of oxygen diffusion. The second hypothesis is the assumption that oxygen diffusion is sensitive to the Fermi energy level change, caused by the heavy doping incorporation.

To investigate how doping can affect the oxygen diffusion, we performed calculations of the diffusion coefficient of monomer and dimer in proximity of the dopant atoms. In other words, we introduce both the dopant and oxygen in supercell at the same time. Two defects were distanced by 15 Å in a 512 Si atoms supercell. The binding between oxygen species and dopant was obtained to be zero. Thus we infer no impact of dopant on ground-state properties of oxygen species.

1. *Geometries*

The effect of dopants on the geometries of the ground-state and transition configurations are listed in Tables I and III for monomer and dimer, respectively. The geometry of the ground-state configurations is not affected by any of tested dopants.

However, significant changes in the transition state geometries were observed. Both B and As presence in the supercell leads to the same changes in monomer geometries. The Si_1-O and Si_3-O bond lengths are increased from ∼3.480 to ∼3.530–3.610 Bohr, while the Si_2-O bond length is reduced from ∼3.370 to ∼3.300 Bohr in both cases. Ge presence does

TABLE III. Geometry parameters of the oxygen dimer configurations (see Fig. 3 for the schemes). The length values are in Bohrs, the angles are in degrees.

doping	Conf.	$\hat{a}$	$\hat{b}$	$\hat{c}$	$\hat{d}$	$\hat{\mathrm{Si}}_{123}$	$\hat{\mathrm{Si}}_{234}$	$\mathrm{Si_1}$-$\mathrm{O_I}$	$\mathrm{Si_2}$-$\mathrm{O_I}$	$\mathrm{Si_3}$-$\mathrm{O_I}$	$\mathrm{Si_2}$-$\mathrm{O_{II}}$	$\mathrm{Si_3}$-$\mathrm{O_{II}}$	$\mathrm{Si_4}$-$\mathrm{O_{II}}$
pristine	GS	142.7	71.6	145.1	60.9	97.2	98.6	3.093	3.053	6.040	3.037	3.088	4.985
B	GS	142.5	70.9	146.2	59.5	98.3	100.2	3.090	3.061	6.090	3.035	3.085	5.090
Ge	GS	142.6	71.0	146.6	59.4	98.2	100.3	3.093	3.067	6.094	3.038	3.083	5.100
As	GS	142.6	71.0	146.6	59.4	98.2	100.3	3.093	3.067	6.095	3.038	3.083	5.101
pristine	TS	88.2	95.7	101.5	79.8	95.0	97.4	3.834	3.257	3.536	3.262	3.244	4.098
B	TS	83.6	99.0	98.1	84.4	95.7	95.6	3.962	3.257	3.357	3.393	3.265	3.936
Ge	TS	83.4	98.7	99.4	82.3	95.8	96.7	3.956	3.261	3.363	3.339	3.256	4.040
As	TS	76.8	102.6	95.6	85.6	99.4	96.7	4.111	3.225	3.298	3.603	3.249	3.769

not affect much the transition state geometry of the monomer (see Fig. 3 for notations). In brief, we observe no impact on GS configurations of both the monomer and the dimer, however doping significantly affect the TS configurations.

2. Migration and binding energies

Recently, we reported the effect of dopants on the migration energies of diffusing oxygen species [42]. These results are listed in Table V. The migration energy of oxygen monomer is reduced by ∼0.4 eV due to the presence of p-type dopants. n-type dopants also lead to a reduced migration energy but in a smaller extent of ∼0.15 eV. Germanium presence does not affect the monomer's migration energy.

The effect of dopants on the dimer's energy barrier has the opposite trends. There is almost no effect of p-type dopants, however, there is slight increase by ∼0.1 eV caused by n dopant and isovalent dopant presence in the supercell.

There are no significant changes in the dimer's binding energy, being about 0.14 eV in all tested cases except Sb dopant. In the latter case, a negative binding energy of −0.39 eV was obtained.

We have shown that p-type doping plays a significant role on monomer's migration energy. In this paper, we aim to further investigate the mechanisms, responsible for the reported reduction in monomer's migration energy.

3. Pre-exponential factors

To have a full picture of diffusing properties and to draw final conclusions, the information about the pre-exponential factor in the diffusion coefficient is crucial. The calculated pre-exponential factor values for representative cases of B, Ge, and As are listed in Table VI. For the dimer case, the calculation of the effective pre-exponential factor at low temperature is derived from Eq. (8). The oxygen monomer concentration was considered to be 10^{18} cm^{-3} in all cases. Note that $D_0(O_2)$ is proportional to the oxygen concentration. Thus the reduction of the latter by one order in magnitude will cause the same one order reduction in the pre-exponential factor.

Boron has an important impact on the migration energy of the monomer, but we only observed a slight change in the prefactor value. The effects of Ge and As are more pronounced. Our calculations suggest that in the Ge-doped case the pre-exponential factor is lower by a factor of 8, whereas As presents a reduction by a factor of 4. The corresponding values are 0.004 and 0.009 cm^{-2} s^{-1} in the case of Ge and As doping, respectively. The doping effect on the dimer's pre-exponential factor has an inverse trend. The isovalent doping nearly has not impact on the pre-exponential factor, whereas arsenic slightly increases it by a factor of 2, and boron reduces it by a factor of 5.

4. Charge transfer mechanism

Prior to discussing the calculated diffusion coefficient as a function of temperature in heavily doped materials, we will consider the charge transfer mechanism in more details. For this purpose, we performed NEB calculations to find the minimum energy diffusion path of oxygen monomer in a 216 Si supercell. We compared the diffusion in the proximity of boron and arsenic dopants with diffusion in a nondoped supercell. The obtained paths as a function of reaction coordinates are represented in Fig. 6. The migration energies obtained with DIIS scheme and using the NEB technique are 2.41 and 2.35 eV, respectively. Such a small difference between energies shows both efficiency of the DIIS technique and the convergence level of a 216 Si supercell with respect to the 512 Si atoms supercell. The slightly lower value obtained using the NEB technique is related to the elastic bands that restrict the images along the migration path. The path of 41

TABLE IV. The effect of biaxial strain, applied in ⟨110⟩ plane, on E_m and D_0 of oxygen monomer diffusion. Strains of ±0.5% applied in ⟨110⟩ plane are chosen as an example, as it gives the maximal effect on migration energy.

Strain	E_m (eV)	$D_0(O_i)$ (cm^2 s^{-1})
−0.5%	2.22	0.002
0.0%	2.29	0.010
+0.5%	2.37	0.009

TABLE V. The calculated migration energies and binding energies of oxygen monomer and dimer when a doping element is inserted as a substitutional atom in the calculation supercell.

dopant	–	B	Al	Ga	Ge	P	As	Sb
$E_m(O)$ (eV)	2.41	2.01	2.04	2.05	2.39	2.26	2.29	2.24
$E_m(O_2)$ (eV)	1.62	1.66	1.63	1.62	1.74	1.75	1.71	1.74
$E_b(O_2)$ (eV)	0.14	0.15	0.15	0.14	0.14	0.14	0.14	−0.39

TABLE VI. Calculated pre-exponential factor values of diffusion coefficients of oxygen monomer and dimer in silicon with or without the presence of a doping element as a substitutional atom in the calculation supercell.

dopant	–	B	Ge	As
$D_0(O)$ (cm^2 s^{-1})	2.9×10^{-2}	3.2×10^{-2}	0.4×10^{-2}	0.9×10^{-2}
$D_0(O_2)$ (cm^2 s^{-1})	7.6×10^{-7}	1.7×10^{-7}	15.0×10^{-7}	7.9×10^{-7}

images resulted in a highly symmetric curve with a transition state situated very close to the middle of the path.

The changes of the barrier height due to the dopants presence agree well with previously obtained values (summarized in Table V). The shapes of the three curves are merged starting from the GS and they start splitting after the inflection point. Let us suggest that the charge transfer appears at the moment of the curves splitting. To analyze the electronic distribution along the path, we mapped the electronic density of an unpaired electron for the cases of B- and As-doped supercells (see Fig. 7). Numbered points correspond to the number label in Fig. 6. The dopant is positioned near the top left corner of the projection, while the oxygen atom is located in the right-hand side. The electronic distribution of the lone unpaired electron clearly indicates that starting from the ground state and up to the image numbered 4, oxygen diffuses as a neutral species. From the point numbered 5 in Fig. 6, the charge is already located around the oxygen. This finding indicates that monomer diffusion in heavily doped silicon is assisted by a charge transfer. This charge is a hole in the B-doped case and an electron in the As-doped case.

The charge transfer mechanism occurs in the dimer diffusion as well, but causes only a slight increase in its migration energy. The reason for that could lie in the electronic configuration of the transition state of the dimer. Contrary to the monomer case, it is less active. During the migration process, two hopping bonds of two oxygen atoms can be neutralized by each other, causing a lower migration barrier, which is less sensitive to the charge transfer mechanism.

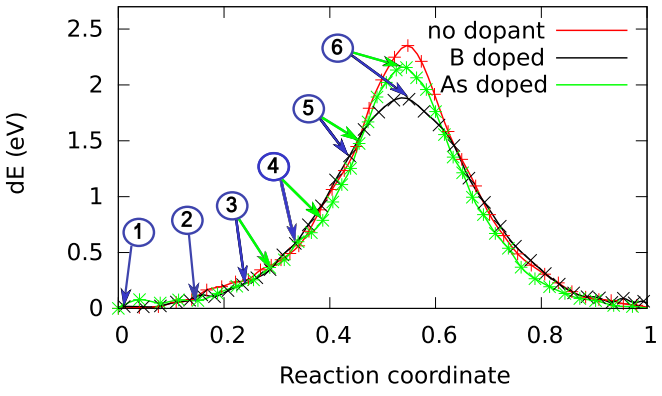

FIG. 6. The 41 images NEB paths of oxygen monomer in 216 Si atoms supercells. Results for B- and As-doped supercells are compared with undoped supercell. Figure 7 illustrates the snapshots of up-down electronic density corresponding to (1) first, (2) fifth, (3) ninth, (4) 13th, (5) 17th, and (6) 21st images of B- and As-doped cases.

IV. DISCUSSION

We have reported migration energy values for the oxygen monomer and dimer in low doped and heavily p- and n-doped silicon, through *ab initio* calculations. They are in excellent agreement with experimental data. The results were obtained in 512 Si supercells by employing a DIIS optimization scheme for the saddle point relaxation as well as the NEB relaxation technique in 216 supercells.

Recently, in 2014, Binder *et al.* [55] have performed an *ab initio* study of oxygen migration path in pristine silicon. They have obtained an asymmetric path for oxygen monomer diffusion slightly lower in energy than the symmetric path. They claim that enough images in the NEB calculation are necessary to obtain the proper asymmetric migration path. The result shown here illustrates that even a higher number of images can stabilize the symmetric path. This result does not contradict the one of Binder *et al.*, but emphases the existence of several oxygen migration paths.

For pristine silicon, the calculated values reproduce the experiments, the monomer diffusion at the high temperature regime and dimer diffusion at the low temperature regime. In addition, our results show that strain cannot affect oxygen diffusivity. However, heavy doping can impact the oxygen diffusivity by electronic interaction, specifically by a charge transfer mechanism. This effect is demonstrated in Fig. 7. Indeed, a dopant belonging to the III column of the periodic table introduces a hole into the supercell. The latter can be spread over a wide area around. The electronic density of this hole is revealed by the $\rho^{\text{unpaired}}(\vec{r})$ map obtained from DFT calculations and represented on top line in Fig. 7. In the case of the n-type dopant, the supercell has also an odd number of electrons. Here, the unpaired electron belongs to the dopant atom and is localized in a smaller sphere around it.

The binding energy between the interstitial oxygen monomer and a dopant, being B or As, is equal to zero in both cases. Note that the distance between two point defects is less that 15 Å as we deal here with 216 Si supercells. These results are in line with the fact that geometry parameters of the interstitial oxygen are the same as in pristine silicon. The potential energy surface has exactly the same shape, according to the shape of the NEB curves. The NEB paths in all three cases, namely pristine, B-containing, and As-containing, are merged in ranges of 0.0–0.4 and 0.6–1.0 of reaction coordinates of Fig. 6.

Once the oxygen approaches the transition state, it becomes electrically active and attracts the electronic density towards itself. This effect is illustrated by the $\rho^{\text{unpaired}}(\vec{r})$ distribution: top and bottom images (5) and (6) on Fig. 7. A hole is attracted in B-doped case and an electron is attracted in As-doped case. Once the oxygen atom overpasses the transition state, the electron goes back to the dopant.

Such a charge transfer mechanism allows reducing the migration energy barrier, if a charge electron detaches easily from its source. In the case of B doping, we obtained a reduction of monomer migration energy by 0.4 eV. However, trying to add a second B in the system leads only to a slight reduction in migration energy of 0.08 eV. Thus we conclude that ∼0.4 eV is the highest possible reduction for the oxygen monomer's migration energy. Our calculations predict the

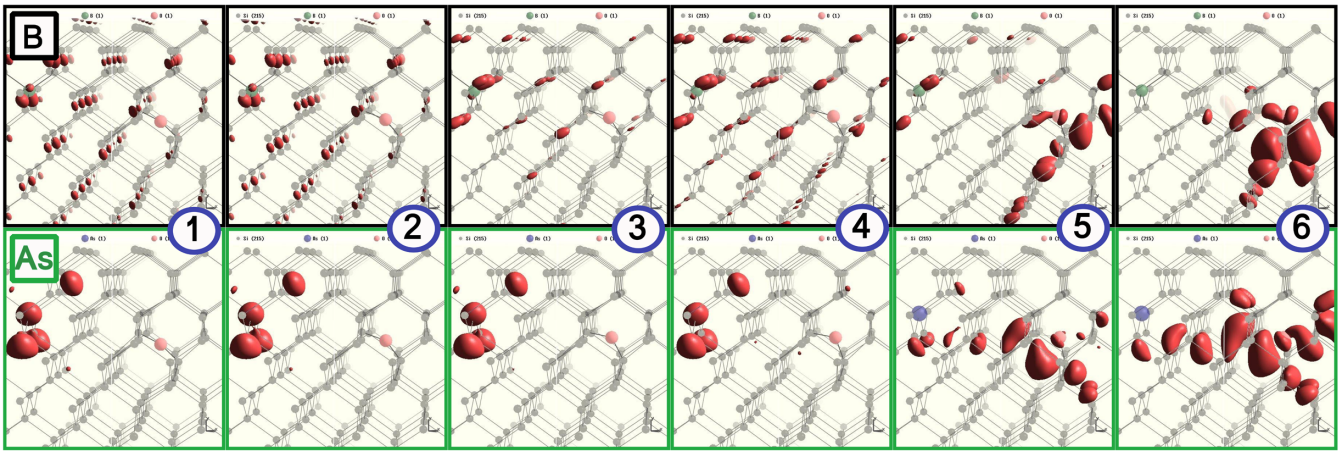

FIG. 7. The up-down electronic density $\rho^{\text{unpaired}}(\vec{r})$ [$\rho^{\text{unpaired}}(\vec{r}) = \rho_{\uparrow}(\vec{r}) - \rho_{\downarrow}(\vec{r})$] mapped along the oxygen monomer migration path for B and As dopant cases (see Fig. 6). Number 1 corresponds to the ground state of oxygen monomer, while number 6 is related with the transition state. The dopant atom is located on the right side of each snapshot, while the migrating oxygen is on the left side. The electron density transfers from the dopant vicinity (numbers 1–4) towards the migrating oxygen (numbers 5 and 6).

same effect on migration energy in the presence of Al and Ga. If the element is a n-type dopant, the charge transfer leads to a smaller reduction of the migration energy of only ∼0.15 eV.

In proximity of p- and n-type dopants, the dimer diffusion is also charge assisted, according to our results. However, we did not register a considerable change of the migration energy in proximity p-type dopants, and we detect only a slight increase of 0.09 eV in proximity of As dopant (see Table V). Doping with germanium does not affect the migration energy of the monomer, however it leads to an increase of 0.12 eV of that of dimer and is similar to the n-doped case.

Finally, the complete comprehension of diffusing properties implies the investigation of the temperature dependence of the calculated diffusion coefficients. In Fig. 8, the calculated diffusion coefficients of the oxygen monomers and dimers are

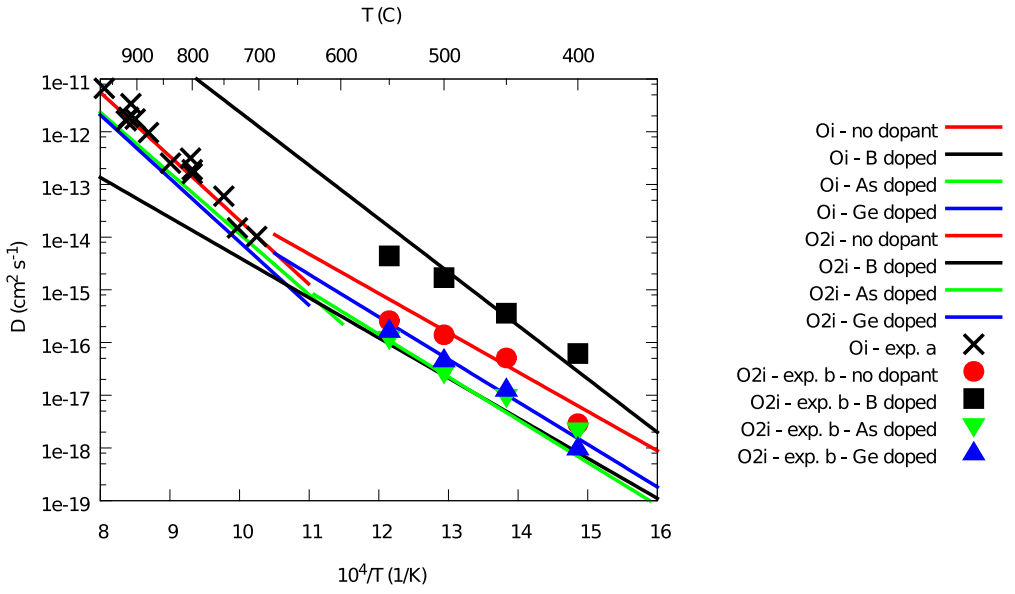

FIG. 8. Overall picture of the oxygen diffusion coefficients, both from experimental data (as represented by dots) and from numerical simulations (represented by lines). Experimental data come from two references: the first one labeled "exp. a" in this figure, features oxygen diffusion at high temperatures [14] and the second one, labeled "exp. b" gives measurements in a lower temperature range for pristine silicon or in the presence of dopants [17]. The simulated diffusion coefficients come from *ab initio* calculations presented in this paper. The solid lines stand for monomer diffusion while dashed lines represent dimer diffusion. The effect of dopants on the diffusion coefficients is represented by different colors, red for undoped cases, black for B-doped, green for As-doped, and blue for Ge-doped cases. The main feature of this figure is the higher diffusion coefficient obtained by simulation for the monomer (black solid line) in the B-doped case, while previously the measured enhancement (black squares) was generally attributed to enhanced dimer diffusion.

plotted together with experimental data from Refs. [14,20,21] with respect to inverse temperature.

First, it is worth to notice that Ge and As doping should affect diffusion coefficients of monomer and dimer in the same extent (green and blue lines in Fig. 8). An impact of both dopants on the migration energy (see Table V) and pre-exponential factor (see Table VI) of oxygen dimer lead to a similar reduction in the diffusion coefficient that fully agrees with experimental trends from Ref. [21]. More specifically, in both cases, a slight increase in migration energies leads to a steeper slope of Arrhenius plot and results in lowered diffusion coefficient of oxygen dimer at low temperatures. At high temperatures, we obtained slightly reduced monomer's diffusion coefficients in proximity of Ge and As. This effect is related with the decrease in pre-exponential factor of monomer with respect to pristine silicon (Table VI), while migration energies are not affected (Table V).

At thermodynamic equilibrium, the diffusion of the oxygen dimer in proximity of boron proceeds with a lower diffusion coefficient (black lines dashed line in Fig. 8), while monomer diffusion is enhanced (solid black line in Fig. 8). Murphy *et al.* [20] in their paper are reporting diffusivity values (see Fig. 6 in Ref. [20]) in a temperature range where the oxygen diffusion is known to be mediated by the oxygen dimer but they observed a significant increase in diffusivity when the sample is heavily B-doped. Assuming an Arrhenius behavior in this regime, one can fit the experimental points and obtain a prefactor and an activation energy. Though the experimental technique cannot give a clue on which mechanism is giving this Arrhenius behavior. On the other hand, using the atomistic simulation results of the present article, assuming a monomer or a dimer mechanism, we show that only the diffusivity of the monomer is increased in this same temperature range, raising monomer diffusivity values in the range of the experimental ones. This result clearly discards the dimer mechanism for B-doped sample as explanation for the diffusivity raise. Although, the calculated prefactor and activation energy for the monomer are still quite different from the fitted experimental ones, the resulting diffusivity are quite similar. This apparent inconsistency suggests that the experimental raise in the diffusivity is a complex combination of mechanisms, where the monomer is playing a key role although it seems to be mitigated by a side mechanism that is not included in the present simulation (e.g., a temperature dependence of the charge transfer mechanism).

This finding raises the question of how monomers diffuse in the high temperature regime in heavily B-doped silicon, since the extrapolation of our enhanced diffusion coefficient to the high temperatures does not match the experimental data (left hand side of the solid black line in Fig. 8). Indeed, recent experiments suggest that "normal" (i.e., not enhanced) diffusion happens at high temperatures in heavily B-doped sample [22,23]. We propose possible reasons for the enhanced monomer diffusion not to happen at elevated temperatures. The first reason can be point defects appearance in concentration of the order of boron atoms. Formed at high temperatures, those defects can trap holes and block the charge assisted migration. The second reason can be a change of conductivity type. As far as p- or n-type semiconductors become intrinsic at high temperatures, charge assisted diffusion can be blocked because of mobile electrons and holes presence in concentrations of the order of dopant atoms.

In the case of hydrogen enriched samples as well as in samples with metallic impurities, we suggest that enhanced oxygen diffusion may happen assisted by a charge, as demonstrated in this article for B-doped silicon. Indeed, weakly binded electrons can participate in the oxygen diffusion process, causing a reduced migration energy. Experimentally, migration energies of about 2 eV have been obtained in hydrogen and metallic impurities presence [24–26]. This value is equal to the calculated migration energy of monomer in proximity of p dopants, and we therefore suspect that charge assisted diffusion can take place in mentioned samples as well.

The enhanced and retarded diffusion, obtained with different techniques for heavily B-doped samples, suggests either enhanced (DLT) or reduced (SIMS out-diffusion) diffusion of oxygen at low temperatures. Our DFT-based calculations support the enhanced diffusion due to the accelerated migration of monomers, which can also result in the enhanced precipitation, recently observed in Ref. [23]. The SIMS out-diffusion profiles, in this case, may indeed result from reduced free oxygen in the sample. Moreover, it was shown that the oxygen out-diffusion profiles are sensitive to surface effects and the oxygen concentration in the bulk [16].

It is worth to notice that at high doping rates a significant amount of dopant atoms can stay precipitated. Apparently, these precipitates may also have an impact on oxygen diffusivity. At the same time, high precipitation rates result in lowered single dopant concentration, which does not affect oxygen diffusion. Therefore the balance between precipitated and nonprecipitated dopants may be the reason of the diversity of results in experiments. However, further investigation is absolutely necessary. Similarly, the boron-oxygen defects may also impact oxygen species' behavior, and therefore is a good direction for further research.

Another controversy is related to Sb doping. The SIMS out-diffusion suggests a reduced diffusivity with an activation energy of about 3.0 eV, while DLT has not detected any pronounced changes. According to our results, among tested elements only Sb impacts the binding energy of the dimer (see Table V), making it unstable and thus impossible to form and diffuse. This suggests that it will preferably diffuse as a monomer with an activation energy of at least 2.5 eV. Furthermore, the trapping of oxygen by Sb may further increase the activation barrier [see Eq. (3)]. If Sb and O atoms are separated by 15 Å, the binding between Sb and O was calculated to be 0.52 eV, raising E_a around 3 eV.

V. CONCLUSIONS

We have thoroughly investigated the diffusion properties of oxygen species, monomers and dimers, through DFT based calculations. We showed that the investigation of the two parameters of diffusion coefficient, namely pre-exponential factor and migration energy, is crucial for this kind of investigation as it allows direct comparing theoretical results with experiment. In our case, we reproduced the experimental results for all doping types.

On one hand, we showed that the effect of strain on the oxygen transport is negligible. On the other hand, we have highlighted a switch in the diffusion mediator. While lowering the temperature favors the oxygen dimer as the primary diffusing species over the slower monomer, p doping is responsible for promoting again the monomer as primary diffusing species. This switch is supported by a charge transfer, reducing the migration barrier while the diffusion prefactor is kept at a high value.

ACKNOWLEDGMENTS

This work was funded by the French National Research Agency through the BOLID Project Projet-ANR-10-HABI-0001. This work was granted access to the HPC resources of TGCC under the allocation 2014-096107 made by GENCI. D.T. thanks CEA-INES for partial funding. Dr. Sebastien Dubois, Dr. Jean-Paul Garandet, and Dr. Jordi Veirman are acknowledged for scientific discussions.

[1] H. Bracht, MRS Bull. **25**, 22 (2000).
[2] R. C. Newman, J. Phys.: Condens. Matter **12**, R335 (2000).
[3] W. K. Tice and T. Y. Tan, Appl. Phys. Lett. **28**, 564 (1976).
[4] S. Hahn, H. J. Stein, S. C. Shatas, and F. A. Ponce, J. Appl. Phys. **72**, 1758 (1992).
[5] G. Kissinger, in *Defects and Impurities in Silicon Materials*, edited by Y. Yoshida and G. Langouche (Springer, Japan, 2016), pp. 273–341.
[6] K. Bothe and J. Schmidt, J. Appl. Phys. **99**, 013701 (2006).
[7] E. N. Sgourou, D. Timerkaeva, C. A. Londos, D. Aliprantis, A. Chroneos, D. Caliste, and P. Pochet, J. Appl. Phys. **113**, 113506 (2013).
[8] H. Fischer and W. Pschunder, *Proceedings of the 10th IEEE Photovoltaic Specialists Conference, Palo Alto, CA* (IEEE, New York, 1973), p. 404.
[9] J. Schmidt and K. Bothe, Phys. Rev. B **69**, 024107 (2004).
[10] V. V. Voronkov and R. Falster, J. Appl. Phys. **107**, 053509 (2010).
[11] J. Adey, J. P. Goss, R. Jones, and P. R. Briddon, Physica B: Condens. Matter **340**, 505 (2003).
[12] X. Yu, P. Chen, X. Chen, Y. Liu, and D. Yang, AIP Adv. **5**, 077154 (2015).
[13] A. Herguth, G. Schubert, M. Kaes, and G. Hahn, *Proceedings of the 21st European Photovoltaic Solar Energy Conference, Dresden, Germany* (WIP Renewable Energies, Munich, 2006), p. 530.
[14] J. C. Mikkelsen, Jr., MRS Proceedings **59**, 19 (1986).
[15] S.-T. Lee, P. Fellinger, and S. Chen, J. Appl. Phys. **63**, 1924 (1988).
[16] S. A. McQuaid, B. K. Johnson, D. Gambaro, R. Falster, M. J. Ashwin, and J. H. Tucker, J. Appl. Phys. **86**, 1878 (1999).
[17] S. Senkader, P. R. Wilshaw, and R. J. Falster, J. Appl. Phys. **89**, 4803 (2001).
[18] V. V. Voronkov, G. Voronkova, A. Batunina, V. Golovina, R. J. Falster, M. Cornara, N. Tiurina, and A. Guliaeva, Solid State Phenom. **156-158**, 115 (2010).
[19] V. Quemener, B. Raeissi, F. Herklotz, L. I. Murin, E. V. Monakhov, and B. G. Svensson, J. Appl. Phys. **118**, 135703 (2015).
[20] J. D. Murphy, S. Senkader, R. J. Falster, and P. R. Wilshaw, Mater. Sci. Eng. B **134**, 176 (2006).
[21] Z. Zeng, J. D. Murphy, R. J. Falster, X. Ma, D. Yang, and P. R. Wilshaw, J. Appl. Phys. **109**, 063532 (2011).
[22] K. Torigoe, J. Fujise, T. Ono, and K. Nakamura, J. Appl. Phys. **116**, 193503 (2014).
[23] J. Will, A. Groschel, E. Bergmann, E. Spiecker, and A. Magerl, J. Appl. Phys. **115**, 123505 (2014).
[24] R. C. Newman, A. K. Tipping, and J. H. Tucker, J. Phys. C: Solid. Stat. Phys. **18**, L861 (1985).
[25] A. K. Tipping and R. C. Newman, Semicond. Sci. Tech. **2**, 315 (1987).
[26] C. Maddalon-Vinante, D. Barbier, H. Erramli, and G. Blondiaux, J. Appl. Phys. **74**, 6115 (1993).
[27] T. Ono, G. A. Rozgony, E. Asayama, H. Horie, H. Tsuya, and K. Sueoka, Appl. Phys. Lett. **74**, 3648 (1999).
[28] M. Pagani, J. Appl. Phys. **68**, 3726 (1990).
[29] K. Wada, Phys. Rev. B **30**, 5884 (1984).
[30] H. Takeno, K. Sunakawa, and M. Suezawa, Appl. Phys. Lett. **77**, 376 (2000).
[31] L. I. Khirunenko, Y. V. Pomozov, M. G. Sosnin, A. V. Duvanskii, N. A. Sobolev, N. V. Abrosimov, and H. Riemann, Physica B: Condens. Matter **404**, 4698 (2009).
[32] U. Gösele and T. Y. Tan, Appl. Phys. A **28**, 79 (1982).
[33] Y. J. Lee, J. von Boehm, M. Pesola, and R. M. Nieminen, Phys. Rev. B **65**, 085205 (2002).
[34] C. Cui, X. Ma, and D. Yang, Phys. Status Solidi **205**, 1148 (2008).
[35] H. Takeno, Y. Hayamizu, and K. Miki, J. Appl. Phys. **84**, 3113 (1998).
[36] J. Adey, R. Jones, D. W.Palmer, P. R. Briddon, and S. Öberg, Phys. Rev. Lett. **93**, 055504 (2004).
[37] M.-H. Du, H. M. Branz, R. S. Crandall, and S. B. Zhang, Phys. Rev. Lett. **97**, 256602 (2006).
[38] L. I. Murin, E. A. Tolkacheva, V. P. Markevich, A. R. Peaker, B. Hamilton, E. Monakhov, B. G. Svensson, J. L. Lindstrom, P. Santos, J. Coutino, and A. Carvalho, Appl. Phys. Lett. **98**, 182101 (2011).
[39] J. Bourgoin, D. Peak, and J. W. Corbett, J. Appl. Phys. **44**, 3022 (1973).
[40] J. C. Bourgoin, J. W. Corbett, and H. L. Frisch, J. Chem. Phys. **59**, 4042 (1973).
[41] D. Peak, J. Corbett, and J. C. Bourgoin, J. Chem. Phys. **65**, 1206 (1976).
[42] D. Timerkaeva, D. Caliste, and P. Pochet, Appl. Phys. Lett. **103**, 251909 (2013).
[43] G. Vineyard, J. Phys. Chem. Solids **3**, 121 (1957).
[44] V. Gusakov, Solid State Phenom. **205-206**, 171 (2014).
[45] J. P. Perdew, K. Burke, and M. Ernzerhof, Phys. Rev. Lett. **77**, 3865 (1996).
[46] M. Krack, Theor. Chem. Acc. **114**, 145 (2005).
[47] L. Genovese, A. Neelov, S. Goedecker, T. Deutsch, S. A. Ghasemi, A. Willand, D. Caliste, O. Zilberberg, M. Rayson, A. Bergman, and R. Schneider, J. Chem. Phys. **129**, 014109 (2008).

[48] E. Bitzek, P. Koskinen, F. Gähler, M. Moseler, and P. Gumbsch, Phys. Rev. Lett. **97**, 170201 (2006).
[49] P. Pulay, Chem. Phys. Lett. **73**, 393 (1980).
[50] E. Machado-Charry, L. K. Beland, D. Caliste, L. Genovese, T. Deutsch, N. Mousseau, and P. Pochet, J. Chem. Phys. **135**, 034102 (2011).
[51] A. Giannattasio, J. D. Murphy, S. Senkader, R. J. Falster, and P. R. Wilshaw, J. Electrochem. Soc. **152**, G460 (2005).
[52] D. Aberg, B. G. Svensson, T. Hallberg, and J. L. Lindstrom, Phys. Rev. B **58**, 12944 (1998).
[53] L. I. Murin, T. Hallberg, V. P. Markevich, and J. L. Lindstrom, Phys. Rev. Lett. **80**, 93 (1998).
[54] J. Coutinho, R. Jones, P. R. Briddon, and S. Öberg, Phys. Rev. B **62**, 10824 (2000).
[55] J. F. Binder and A. Pasquarello, Phys. Rev. B **89**, 245306 (2014).